Inorganica Chimica Acta 459 (2017) 131–142

Contents lists available at ScienceDirect

Inorganica Chimica Acta

journal homepage: www.elsevier.com/locate/ica

Research paper

Counterion effect on the spin-transition properties of the second generation iron(III) dendrimeric complexes

N.E. Domracheva [a,*], V.E. Vorobeva [a,b], V.I. Ovcharenko [c], A.S. Bogomyakov [c], E.M. Zueva [b,d], M.S. Gruzdev [e], U.V. Chervonova [e], A.M. Kolker [e]

[a] Zavoisky Kazan Physical-Technical Institute, Russian Academy of Science, Sibirsky Tract 10/7, 420029 Kazan, Russia
[b] Kazan Federal University, Kremlyovskaya St. 18, 420008 Kazan, Russia
[c] International Tomography Center SB RAS, Institutskaya 3a, 630090 Novosibirsk, Russia
[d] Kazan National Research Technological University, K. Marx Str. 68, 420015 Kazan, Russia
[e] G.A. Krestov Institute of Solution Chemistry, Russian Academy of Science, Akademicheskaya St. 1, 153045 Ivanovo, Russia

ARTICLE INFO

Article history:
Received 16 November 2016
Received in revised form 6 February 2017
Accepted 7 February 2017
Available online 9 February 2017

Keywords:
Iron(III) complex
EPR spectroscopy
Spin-crossover
Magnetic susceptibility
Dendrimers

ABSTRACT

The magnetic properties and the influence of counterions on the spin crossover properties of two novel Fe(III) dendrimeric complexes of the second generation, namely $[Fe(L)_2]^+X^-$, where L = 3,5-di(3,4,5-tris(tetradecyloxy)benzoyloxy)benzoyl-4-oxy-salicylidene-N'-ethyl-*N*-ethylenediamine X = Cl^- (**1**), ClO_4^- (**2**), have been studied for the first time by magnetic susceptibility measurements and electron paramagnetic resonance (EPR) method in a wide (4.2–300 K) temperature range. EPR results showed that compound **1** contains about 98% of high-spin (HS, $S = 5/2$) and ~2% of low-spin (LS, $S = 1/2$) Fe(III) centers, and undergoes an antiferromagnetic ordering below 7 K. The EPR integrated intensity of a broad line ($g \approx 2$), corresponding to the HS iron(III) centers, passes through a broad maximum at $T_{max} \approx 100$ K, which is indicative of short-range correlation effects. The anomalous broadening of this EPR line at low temperatures with the critical exponent $\beta = 1.5$ upon approaching the long-range ordering transition ($T_N^{EPR} = 7$ K) from above indicates the quasi-two-dimensional antiferromagnetic nature of magnetism in complex **1**. The spin-crossover effect is completely suppressed in compound **1**. The complex with ClO_4^- counterion demonstrates a different magnetic behavior. EPR data showed that compound **2** contains about 77% of LS and ~23% of HS Fe(III) centers at $T_N^{EPR} = 10.2$ K. It displays a partial spin crossover ($S = 5/2 \leftrightarrow 1/2$) above 150 K and undergoes the antiferromagnetic ordering below 10.2 K. The obtained results and the results of DFT calculations allowed us to conclude that a bilayered packing with a chain structure of Fe(III) centers in ionic bilayers is formed in compound **1**, whereas a dimeric structure of Fe(III) centers is formed in compound **2**. Thus, the ability of the counterion to form an effective network of hydrogen bonds and its size define the packing motif of the $[Fe(L)_2]^+$ complexes. Therefore, the replacing of the counterion has a significant impact on the magnetic properties of the compound.

© 2017 Elsevier B.V. All rights reserved.

1. Introduction

The spin-crossover (SCO) phenomenon, where spin states may be switched reversibly between low-spin (LS) and high-spin (HS) configurations by external stimuli such as temperature, pressure and more rarely light irradiation, termed the LIESST effect [1–7], can occur in transition metal complexes with a d^4–d^7 electron configuration [1–4]. In particular, the light-induced excited spin-state trapping (LIESST effect), which induces conversion of a LS state to a HS state by means of light irradiation, has attracted considerable interest. Among the most extensively studied SCO materials are complexes of iron(II) (d^6) [8–10] and iron(III) (d^5) [11], which have caused the interest of many researchers as potential multifunctional materials in fields such as molecular electronics, memory storage, sensors and photoelectric devices [12–15]. However, such applications require that the spin transition occurs abruptly at ambient temperature (ideally room temperature) and with wide thermal hysteresis (for the memory effect) [16,17].

In the case of iron(III), which has a d^5 electron configuration, the transition occurs from a high spin state ($^6A_1$, $S = 5/2$) to a low spin state ($^2T_2$, $S = 1/2$) [18,19]. Iron(III) compounds, compared to the iron(II) systems, have the advantage of generally being air stable and thus would be expected to be more amenable to processing

* Corresponding author.
E-mail address: ndomracheva@gmail.com (N.E. Domracheva).

http://dx.doi.org/10.1016/j.ica.2017.02.008
0020-1693/© 2017 Elsevier B.V. All rights reserved.

in any future devices. The hysteresis in the SCO complexes is the result of strong interactions between the SCO centers and it is achieved either through coordination bonds or more commonly supramolecular interactions [20]. The intra- and intermolecular interactions strongly modify the SCO properties. The nature of the complex, intermolecular hydrogen bonds and π-π interactions, solvent molecules, and counterions play a predominant role in the SCO process.

Coordination polymers are declared as the most promising SCO materials for applications [21–23]. The so-called coordination polymers are the SCO complexes with infinite one- or two-dimension (1D, 2D) networks [24]. These systems exhibit enhanced cooperative properties due to strong covalent bonds. In this context, we turned our attention to the dendritic macromolecules capable of organizing themselves in low-dimensional columnar assemblies [25] or into ordered supramolecular structures [26]. One may expect that dendritic macromolecules when precisely organized will generate a long-range cooperation phenomenon. Therefore, our idea was as follows: to insert the cationic SCO iron(III) complex in the focal point (core) of dendrimer molecule and thus to create a new dendritic SCO material with enhanced multifunctional properties. Such a strategy has already demonstrated its beneficial results [27]. Due to this strategy, a new multifunctional material was obtained, in which SCO phenomenon, magnetoelectric effect and long-range magnetic order coexist together. Furthermore, a new physical phenomenon was discovered in this material: magnetic-ferroelectric crossover, where the change in the spin state ($S = 1/2 \Leftrightarrow 5/2$) of iron(III) ion is accompanied by a change in the electric polarization of iron(III) ion [27].

Although the SCO phenomenon is of purely molecular origin, its macroscopic manifestation in the solid state stems from the intermolecular interactions between the spin transiting centers of the material [12]. Furthermore, it is well documented that subtle changes in the crystal packing can give rise to drastic changes in the macroscopic SCO properties of very similar spin transiting Fe (III) centers [28]. The counterions and lattice-solvent molecules have also a significant effect on the spin-transition properties of the material [29,30]. In addition, a change in counterions very often results in an annihilation of the SCO properties due to slight structural variations able to modify the ligand-field strength or form a completely different structure. Consequently, their influence on the spin transition is very difficult to investigate. So far, only a few iron(III) compounds of general formula [Fe(R-SalEen)$_2$]X with bis(tri-dentate) R-SalEen ligands (SalEen = *N*-ethyl-*N*-(2-aminoethyl) salicylaldiminate, R = H, 3-OMe, 4-OMe, 5-OMe, 3-OEt) and various counterions (X = ClO_4^-, NO_3^-, PF_6^-, BPh_4^-) have been reported in the literature [28,31,32]. These compounds have demonstrated a wide variety of SCO properties, ranging from complete to incomplete and from gradual to abrupt spin transitions. For example, the [Fe(3-OMe-salEen)$_2$]PF_6 complex showed an abrupt spin transition at 164 K with a thermal hysteresis loop of 2–4 K.

Herein, we report the magnetic properties of two novel Fe(III) dendrimeric spin crossover complexes based on the SalEen ligand with Cl^- (**1**) and ClO_4^- (**2**) counterions. We continue to study a new series of SCO Fe(III) dendrimeric compounds. Recently, we reported on the magnetic properties of the first representative of this family, the SCO Fe(III) complex with PF_6^- anion [33]. In this compound, EPR spectroscopy revealed the existence of antiferromagnetic (AF) dynamic spin clusters in the paramagnetic phase [33]. The motivation of this work was to determine the influence of counterions on the magnetic properties of the SCO Fe(III) dendrimeric complexes and understand the nature of antiferromagnetic (AF) dynamic spin clusters, since their behavior is more distinctly observed in the iron(III) dendrimeric complex with chlorine counterion (**1**).

2. Results and discussion

2.1. Synthesis and characterization of compounds

The iron(III) bis[3,5-di(3,4,5-tris(tetradecyloxy)benzoyloxy) benzoyl-4-oxy-salicylidene-N'-ethyl-N- ethylenediamine] complexes with chlorine and perchlorate anions were prepared in accordance with Scheme 1 in a similar way as described in [34,35]. The ligand precursor 3,5-di[3,4,5-tris(tetradecyloxy)benzoyloxy]-benzoyl-4-oxy-2-hydroxybenzaldehyde was prepared in accordance with references [35,36]. To avoid some impurity all solutions of iron (III) salts were freshly prepared and filtered through Teflon™ filters (0.200 μ) before used.

Compounds **1** (Cl^-) and **2** ($ClO4^-$) were characterized by elemental analysis, gel permeation chromatography, infrared (IR), NMR spectroscopy and MALDI-ToF-MS method [34]. The results of these methods allowed one to conclude that each of the compounds is a monocationic bis(ligand) Fe(III) complex of formula, $[Fe(L)_2]^+X^-$ (X = Cl^-, ClO_4^-), where iron(III) atom has a pseudooctahedral N_4O_2 coordination core formed by four nitrogen and two oxygen atoms of two tridentate ligands. The schematic model of the complex is given in Scheme 1. X-ray diffraction data obtained for the $[Fe^{III}(SalEen)_2]ClO_4$ analogue without dendritic periphery [28] showed that bis-tridentate ligands are coordinated in a meridional (*mer*) configuration. DFT calculations carried out for the full complex with dendritic environment confirmed that *mer* configuration of ligands is energetically most preferable (see Section 2.4 for details). Such a model of coordination for polyhedron allows the formation of dimeric or chain structure, where neighboring complexes are linked by hydrogen bonds between the amine groups of the SalEen ligands [28,37] and the counterions.

2.2. Magnetic susceptibility data

The temperature dependencies of the effective magnetic moment (μ_{eff}) of compounds **1** and **2** are presented in Fig. 1 in the range (4–300 K). The value of ca. 2.0 μ_B is characteristic of the Fe(III) ions in the low-spin (LS) state, while the value of 5.91 μ_B corresponds to the Fe(III) ions in the high-spin (HS) state.

The magnetic susceptibility data for compound **1** show a gradual decrease in $\mu_{eff}(T)$ behavior from 5.75 μ_B at 300 K to 5.12 μ_B at 50 K and a sharp decrease to 2.93 μ_B when the sample temperature is less than 50 K. Using the relation (1)

$$\mu_{eff}^2 = x\mu_{eff,HS}^2 + (x-1)\mu_{eff,LS}^2, \quad (1)$$

where $\mu_{eff,HS} = 5.91$ μ_B and $\mu_{eff,LS} = 2.0$ μ_B are assumed and x is the fraction of HS molecules, we can conclude that complex **1** at room temperature contains about 95% of HS and 5% of LS Fe(III) molecules. The decrease in μ_{eff} on cooling may be due to the spin transition, the antiferromagnetic (AF) exchange interactions between Fe (III) centers or the contribution from the zero-field splitting parameter (D). A plot of the inverse magnetic susceptibility (χ^{-1}) versus T for **1** (Fig. 2a) indicates that magnetic susceptibility follows the Curie-Weiss law practically in the whole temperature range with the Weiss constant $\theta_1 = -17.2$ K, indicating the presence of AF spin-exchange interactions. Since the deviation from the Curie-Weiss law is not observed, we can conclude that spin crossover does not take place in complex **1**. The zero-field splitting is not responsible for the decrease in μ_{eff}, since the contribution from the zero-field splitting parameter (D) to the Weiss constant is small [38]. Thus, we may conclude that the decrease in μ_{eff} is caused by AF spin-exchange interactions between Fe(III) ions.

The substitution of Cl^- with ClO_4^- counterion leads to a dramatic change in the $\mu_{eff}(T)$ behavior as illustrated in Fig. 1. Compound **2** exhibits a gradual decrease in μ_{eff} from 3.02 μ_B at 300 K to 2.88 μ_B

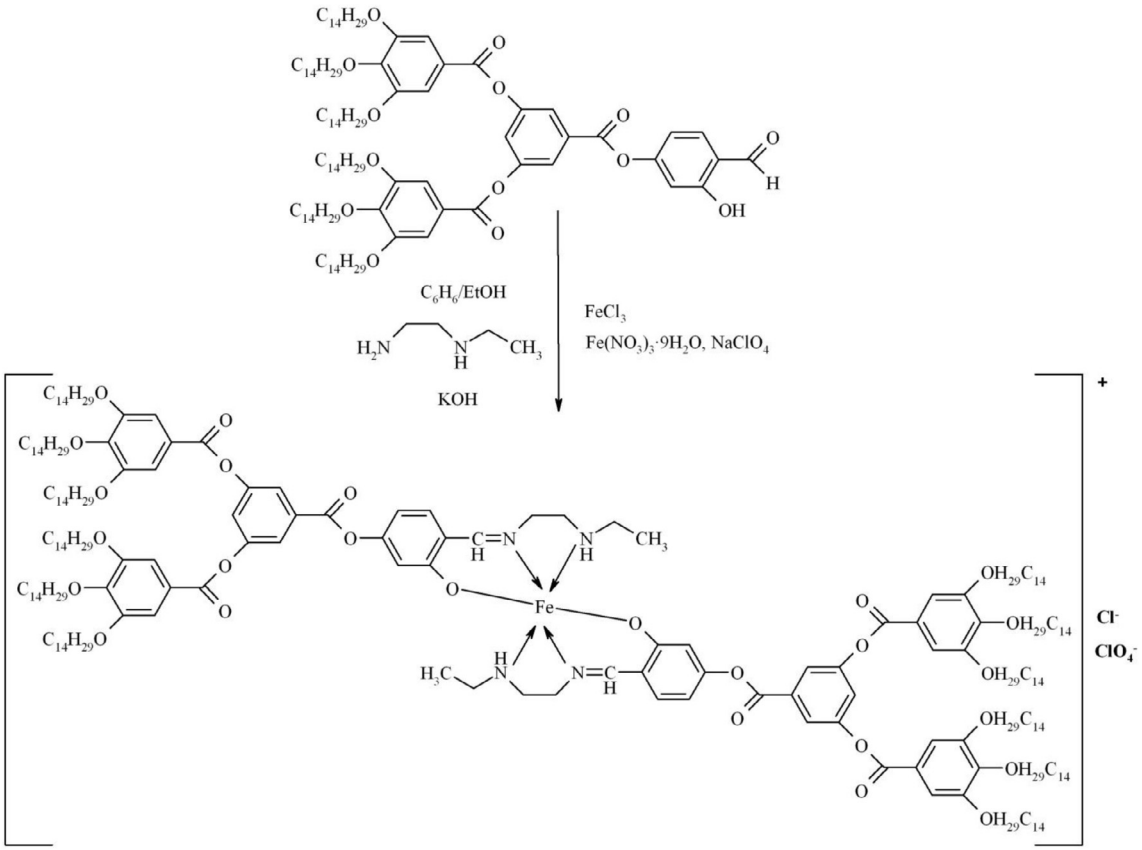

Scheme 1. Schematic representation of the synthetic procedure and schematic model of Fe(III) compounds with Cl^- and ClO_4^- counterions.

at 140 K, practically a plateau from 2.88 μ_B at 140 K to 2.85 μ_B at 30 K, and a sharp decrease to 2.72 μ_B at 5 K. Using the relation (1), we can conclude that complex **2** at room temperature contains about 83% of LS and 17% of HS Fe(III) molecules. A plot of the inverse magnetic susceptibility (χ^{-1}) versus T for **2** (Fig. 2b) shows that magnetic susceptibility follows the Curie-Weiss law at lower temperature with Weiss constant $\theta_2 = -3.8$ K, indicating the presence of AF spin-exchange interactions, and deviates from this law at higher temperature, demonstrating the presence of incomplete SCO.

Thus, it can be concluded that the most Fe(III) ions are in the HS state in complex **1** and SCO effect is completely suppressed in it, while complex **2** shows a gradual, incomplete SCO at high temperature and the most Fe(III) centers are in the LS state. However, AF exchange interactions between the neighboring Fe(III) centers exist in the both compounds. To confirm these conclusions, EPR measurements have been carried out.

2.3. Electron paramagnetic resonance measurements

EPR is a powerful method for studying the SCO effect, since EPR gives information about the existence of LS and HS fractions in the compound and their evolution with temperature. Fig. 3 shows the temperature variation of the X-band EPR spectra ($h\nu = 0.3$ cm^{-1}) for a powder complex **1** in the temperature range (4.2–300 K).

EPR spectra can be seen to demonstrate the presence of three types of iron(III) centers in the sample: two types of HS ions and one of LS. The $g_{eff} = 4.2$ signal and a small line with $g = 9.6$ on the left wing of this signal (Fig. 3, $T = 4.3$ K) belong to the HS iron ions with a strong ($D > h\nu = 0.3$ cm^{-1}) low-symmetry ($E/D \sim 1/3$) crystal field acting on the iron ion, where the line with $g = 4.2$ arises from the middle of the three Kramer's doublet and a weak signal with $g = 9.6$ appears from the lower Kramer's doublet [39,40] (I-type of HS centers). The broad resonance line with $g \sim 2$ which typical for HS Fe(III) ions with a weakly distorted octahedral environment, corresponds to the HS centers of the II-type and demonstrates very interesting features. The behavior of these HS centers, as will be shown below, is similar to the behavior of the same centers in compound with PF_6^- counterion [33]. These centers are packed in a chain forming a layered structure as established in [33]. The LS Fe(III) ions give the anisotropic EPR signal with magnetic parameters: $g_\perp = 2.21$ and $g_\parallel = 1.93$.

The temperature dependence of the EPR lines integrated intensity (I) is one of the sources of information about the spin transition process. The magnetic behavior of compound **1** reflected by the temperature dependencies of I versus T of the whole EPR spectrum is shown in Fig. 4a, where the EPR lines integrated intensity (I) was obtained by numerical double integration of the spectra. One can see that the temperature dependence of I has a complicated, two-step behavior: it reaches the maximum at 7 K and then drops to the minimal value at about 30 K in the first temperature interval (4.2–30 K) and further passes through a broad maximum at $T_{max} \approx 100$ K in the second temperature interval (30–300 K) (Fig. 4a). It should be noted that a more precise maximum is observed in the curve I vs. T for Fe(III) complex with Cl^- counterion as compared to the complex with PF_6^- counterion [33]. Moreover, the position of this maximum shifts towards lower temperatures from $T_{max} \sim 259$ K to $T_{max} \approx 100$ K with a change in the counterion from PF_6^- to Cl^-.

Let us try to understand the origin of the anomalous behavior of I in compound **1**. For this purpose, the temperature dependencies of the EPR lines integrated intensity were examined for each type of Fe(III) centers separately. The analysis of the EPR signals for each type of iron centers was based on the procedure of fitting of the

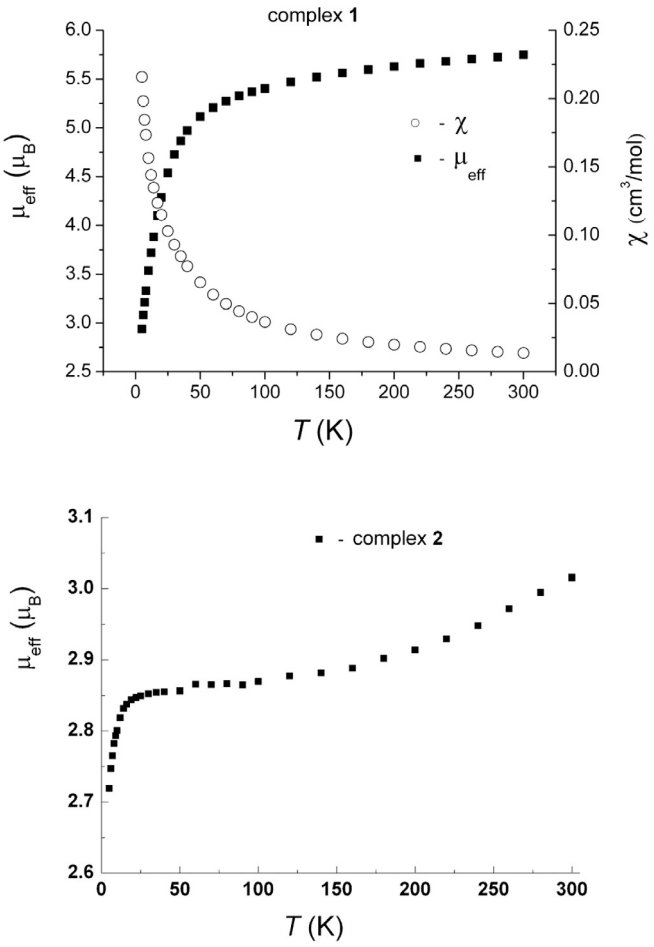

Fig. 1. Temperature dependencies of μ_{eff} vs. T for the compounds **1** and **2**.

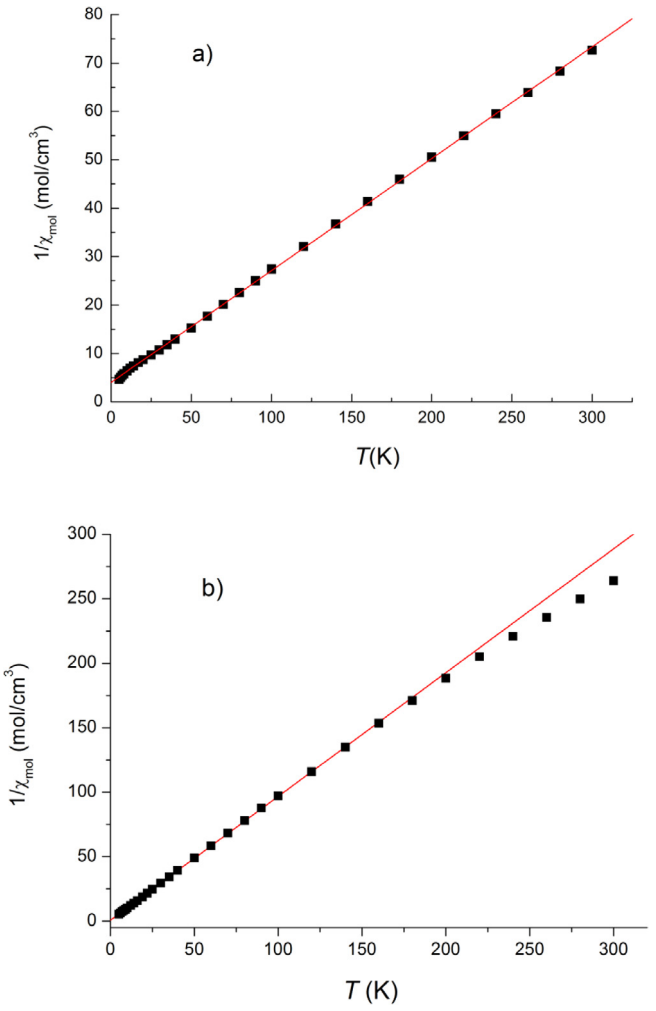

Fig. 2. The inverse magnetic susceptibility of complex **1** (a) and complex **2** (b). The solid straight line represents the Curie-Weiss law with the Curie-Weiss temperature of −17.2 K and −3.8 K for **1** and **2**, respectively.

model spectrum to the observed experimental one. To fit the EPR spectra written in the numerical format, we used a standard Easy-Spin-EPR spectrum simulation program. The simulated by such way EPR spectra are shown in Fig. 3. A broad resonance signal at $g \sim 2$ was satisfactorily described by a single Lorentzian. Fig. 4b–d show the temperature variation of the EPR lines integrated intensities (I) for the HS centers of the I- (I_{HS_I}) and II- (I_{HS_II}) types and LS centers (I_{LS}), respectively. The spectra were fitted with the following magnetic parameters: $g = 2.0$, $D = 0.42$ cm^{-1}, $E = 0.1$ cm^{-1} for the I-type HS centers and $g_{\perp} = 2.21$, $g_{\parallel} = 1.93$ for the LS Fe(III) centers, the values of which are independent of temperature. The temperature behavior of EPR parameters (g-factor, linewidth and integrated intensity) of the II-type HS centers will be considered below.

As can be seen, I_{HS_I} and I_{LS} demonstrate a sharp maximum at $T_N = 7$ K in the first temperature interval 4.2–30 K. The appearance of maximum on the curves shows that LS iron centers as well as HS_I ones are coupled by antiferromagnetic (AF) exchange interactions. It should be noted that the contribution of the zero-field splitting parameters (D, E) does not lead to the appearance of maximum on the curve of the temperature dependence of the paramagnetic susceptibility, as shown in [38]. Above 7 K, the temperature dependencies of I_{HS_I} and I_{LS} follow the Curie-Weiss law. Spin-crossover effect for this type of Fe(III) dendrimeric complexes must be observed above 160 K, as shown in [33]. As seen from the Fig. 4b–d, the number of LS and HS centers decreases in this range (160–300 K) with increasing temperature. This fact indicates that a spin transition (HS ↔ LS) does not take place in compound **1**.

The temperature dependence of I for HS centers of the II-type (I_{HS_II}) behaves in a completely different way, compared to I_{HS_I} and I_{LS}, and demonstrates a broad maximum at $T_{max} \approx 100$ K in the second temperature interval (Fig. 4c). According to the literature data [41], a broad maximum in I_{HS_II} indicates the formation of a magnetic short-range correlation regime, and appearance of a broad maximum is an evidence of low-dimensional AF behavior of the magnetic system. The temperature dependencies of the effective g-factor and line with (ΔH) of this broad line (Fig. 4c) also confirm a low-dimensional behavior of the magnetic system. According to the ratio of the integrated intensities of EPR signals at 100 K, the number of HS centers of the II-type is about 94%, whereas the number of HS centers of the I-type and LS centers is about 4.3% and 1.7%, respectively. Thus, complex **1** consists essentially of HS centers of the II-type and these centers, as will be shown below, are packed in a chain forming a layered structure. Two other types of Fe (III) centers (which are only 6%) probably belong to the ends of chains.

In order to explain the temperature dependence of the EPR integrated intensity, g-factor and width of this broad line corresponding to the HS iron(III) centers of the II-type, let us consider the structural organization of these centers. It is not possible to grow a crystal and to get accurate crystallographic data for such a highly branched dendrimeric compound. However, a similar behavior of I_{HS_II} versus T for compound **1** and complex with PF_6^- counterion

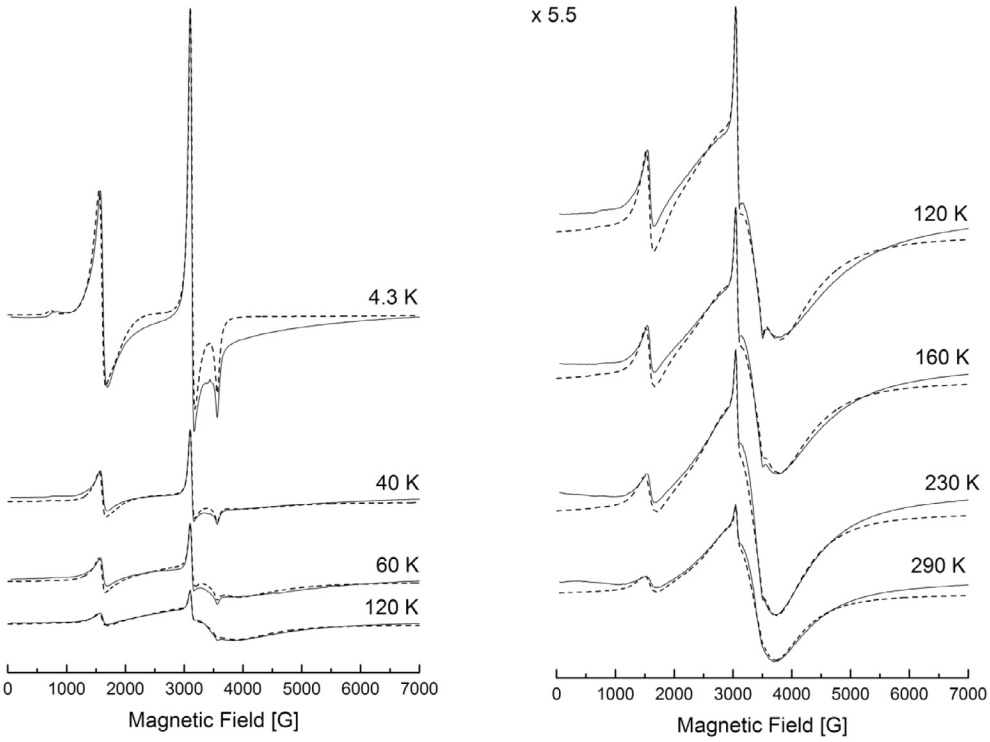

Fig. 3. Temperature profile of the X-band EPR spectra of compound **1** with Cl^- counterion. The dashed lines show the theoretical EPR spectra. Spectra in the temperature range (120–290 K) are recorded at higher amplification (×5.5) in comparison with spectra in the range (4.3–120 K.)

[33] allows us to suggest that HS iron(III) centers of the II-type form chains in layers. Let us turn our attention to the types of structural motifs that can be formed in a similar Fe(III) compounds without dendritic periphery. X-ray diffraction data showed that $[Fe^{III}(SalEen)_2]^+$ cations are packed in a chain forming a layered structure in $[Fe^{III}(SalEen)_2]^+ClO_4^-\cdot 0.5H_2O$ [28] and linked into dimers in $[Fe^{III}(SalEen)_2]^+ClO_4^-$ [28,37], wherein anions are located between the cationic $[Fe(SalEen)_2]^+$ fragments. According to these data, HS iron(III) centers of the II-type should be a quasi-low-dimensional antiferromagnetic system, where neighboring cationic iron complexes are packed head-to-head by means of hydrogen bonds between amine groups and Cl^- counterions, forming a bilayered structure, and bulky dendron substituents well isolate these bilayers from each other. DFT calculations (see Section 2.4 for details) allow us to propose the structure of ionic bilayers in compound **1** (Fig. 5).

In a framework of this concept, one can assume that the broad line (corresponding to the II-type of HS iron centers) originates from a low-dimensional antiferromagnetic system of HS Fe(III) ions. Then, a broad maximum (Fig. 4c) in the temperature dependence of I_{HS_II} versus T characterizes the low-dimensional antiferromagnetic behavior and indicates the short-range correlation effects in the layers of FeN_4O_2 octahedra [41]. The shift of g-factor (Fig. 4c) below ~100 K characterizes the growing role of short-range magnetic correlations. The line broadening (Fig. 4c) on approaching a long-range ordering transition from above is treated as the critical behavior due to the slowing down of spin fluctuations on approaching the critical temperature [42–44]. In this case, the temperature variation of the EPR line width (ΔH) can be described as [41]:

$$\Delta H(T) = \Delta H^* + A\left[\frac{T_N^{EPR}}{T - T_N^{EPR}}\right]^{\beta}, \quad (2)$$

where the first term ΔH^* describes the high-temperature exchange narrowed line with, which is temperature independent, A is an empirical parameter, while the second term reflects the critical behavior with T_N^{EPR} being the temperature of the order-disorder transition and β – the critical exponent. According to the Kawasaki approach [43], the critical exponent can be expressed as $\beta = -[1/2(7+\eta)\nu - 2(1-\alpha)]$, where ν describes the divergence of correlation length, η is a critical exponent for the divergence of static correlations, and α reflects divergence of the specific heat. For a three-dimensional (3D) Heisenberg antiferromagnet [43], β is equal to 1/3. In the case of magnetic systems with lower dimensionality, the critical exponent becomes equal to $\beta = 3/2$ and $\beta = 7/4$ for 2D and 1D system, respectively. In Fig. 6, the solid line superimposed on experimental data represents a least-square fit of the experimental data for the broad line according to Eq. (2) for one-(1D), two-(2D) and tree-dimensional (3D) systems, respectively.

As can be seen, the value $\beta = 1.5$ is slightly better describes the experimentally observed values.

Thus, compound **1** can be regarded as quasi-two-dimensional antiferromagnetic (AF) from the magnetic viewpoint, where cationic HS, $S = 5/2$ iron complexes are packed in a chain forming a layered structure. These AF $S = 5/2$ chains define the magnetic behavior of compound **1** at high temperature and produce the correlation maximum in $I_{HS\_II}(T)$ dependence.

In the case of antiferromagnetic Heisenberg $S = 5/2$ chain, the position of the maximum of magnetic susceptibility (that is proportional to the EPR lines integrated intensity) defines the exchange interaction parameter J_{intra} within the chain through the expression [45]:

$$\frac{k_B[T(\chi_{max})]}{|J_{intra}|} = 10.6 \quad (3)$$

In accordance with the structural features of complex **1**, the dominant magnetic exchange interaction is realized within the chains. The estimation of antiferromagnetic exchange interaction parameter according to Eq. (3) gives $J_{intra} \approx 9.4$ K.

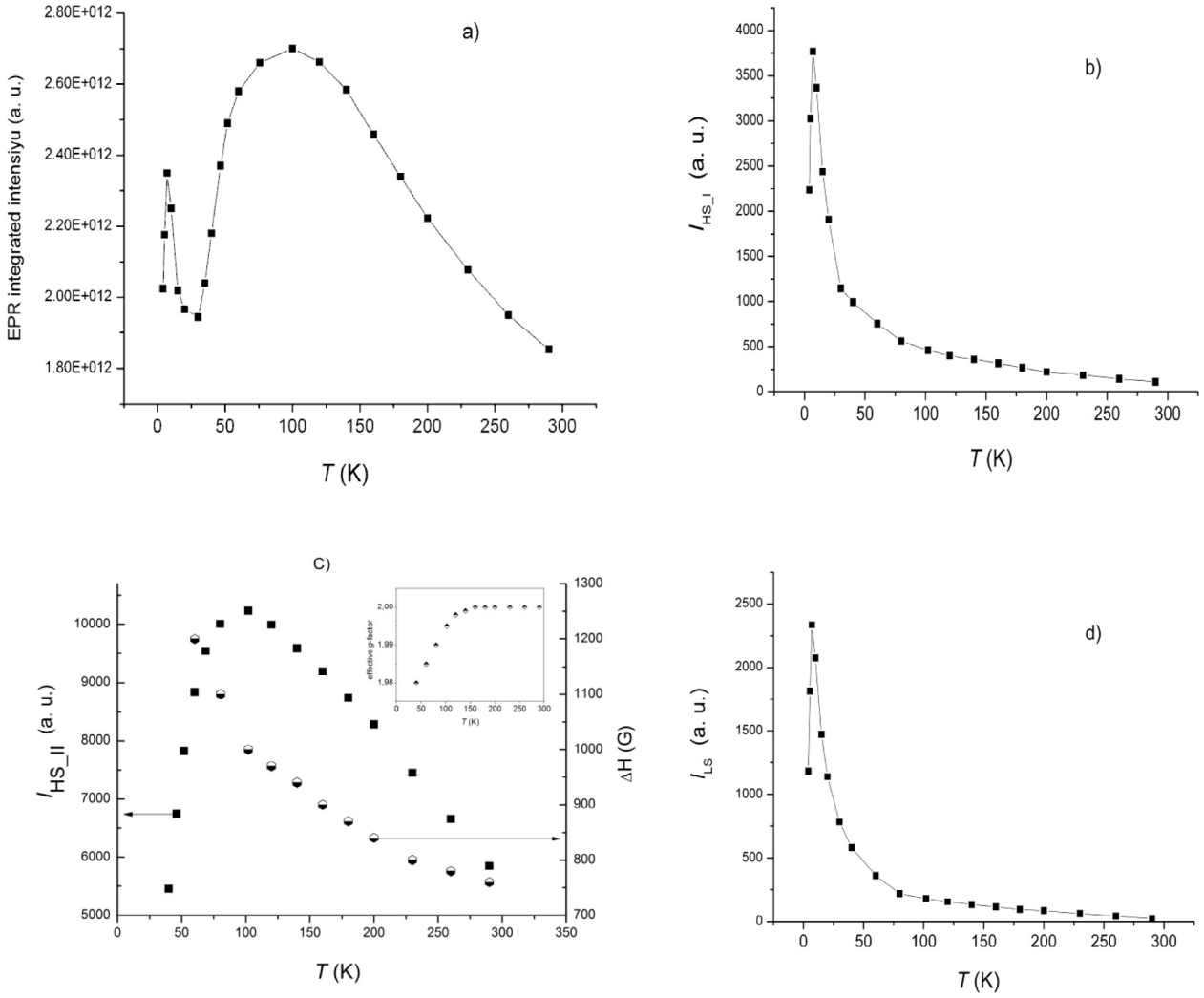

Fig. 4. The temperature dependencies of the EPR lines integrated intensities of the whole EPR spectrum (a), of the I-type HS iron(III) centers (b), of the II-type HS iron(III) centers (c) and of the LS iron(III) centers (d) of the compound **1**.

This value can be determined more precisely using the model of classical linear chains. For this purpose, the experimental data of I_{HS_II} versus T were calculated according to the well-known expression (Eq. (4)) for linear chains of classical spins [46]:

$$\chi = \frac{NS(S+1)g^2\mu_B^2}{3kT} \times \frac{1+u(K)}{1-u(K)}; \quad (4)$$

where $u(K) = \coth K - 1/K; K = -\frac{2JS(S+1)}{kT}$, J is based on the spin-Hamiltonian $H = 2J\sum_{nm} S_i S_j$ with $S = 5/2$ and J is defined as positive for antiferromagnetic coupling. As shown in Fig. 7, the best least-squares fits of the experimental data led to $J_{intra.} = 11.6$ K. As you can see, a good agreement is observed with high-temperature data, but the agreement with low-temperature data (below 80 K) is not satisfactory, which is probably due to the presence of interchain antiferromagnetic interactions.

The value of interchain interaction, $J_{inter.}$, can be estimated according to [47]:

$$\exp\left(\frac{2 \cdot J_{intra}}{k_B T_N}\right) = \frac{4 + Z\eta}{Z\eta} \quad (5)$$

where $\eta = J_{inter.}/J_{intra.}$ and Z is the number of nearest-neighboring chains ($Z = 2$). This expression gives the estimates $\eta = 0.08$ and $J_{inter.} \approx 0.9$ K.

A comparison of the temperature dependencies of the static magnetic susceptibility (Fig. 1a) and the EPR integrated intensity I_{HS_II} (Fig. 4c) shows large differences, especially in the high temperature range (30–300 K). These differences in behavior were observed for the first time in [48] and this can be explained by regarding that I_{HS_II}, in contrast to the static magnetic susceptibility, reveals dynamic spins at the EPR spectrometer frequency (~9.4 GHz). These dynamic spins of short-range ordering are observed only on a short time scale ($\tau = 1/\nu \sim 10^{-10}$ s) and could not be detected by static magnetic measurements ($\tau \sim 100$ s). Thus, the results of our work clearly show that antiferromagnetic short-range correlations act as these dynamic spins. Antiferromagnetic correlations in the complex **1** may have a fast dynamic (fluctuating) nature [49], and, therefore, can't be detected by static magnetic measurements.

Let us consider now the EPR results obtained for complex **2**. Fig. 8 shows the variation of the X-band EPR spectra of the powder sample with temperature. As can be seen, only two signals are observed in the EPR spectra of complex **2**: a low-field signal with $g_{eff} = 4.2$, which belongs to the HS Fe(III) centers with a strong ($D > h\nu = 0.3$ cm^{-1}) low-symmetry ($E/D \sim 1/3$) crystal field, and the axial signal characterized by parameters: $g_\perp = 2.21$ and $g_\parallel = 1.93$, which corresponds to the LS Fe(III) centers.

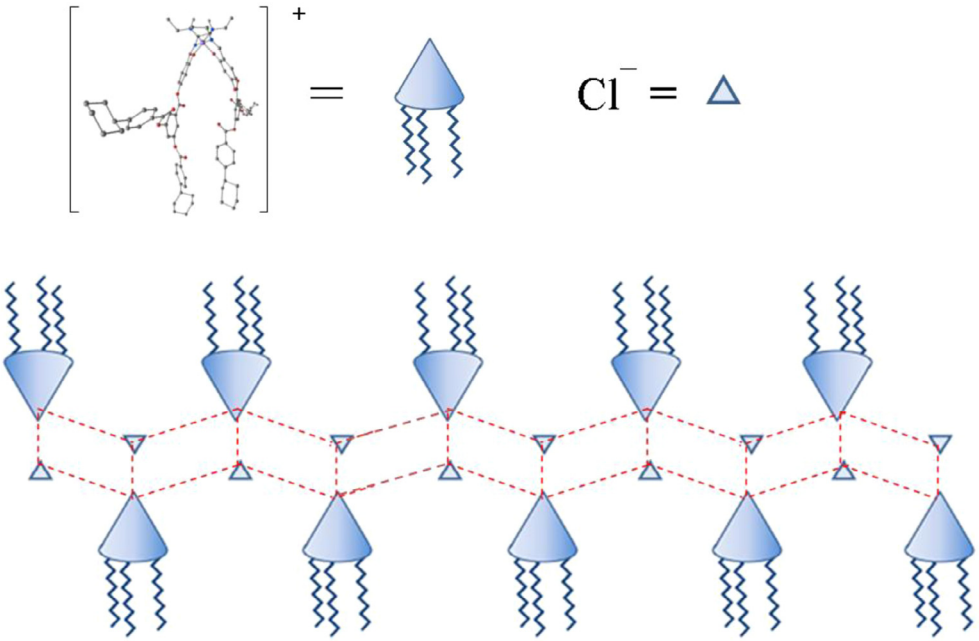

Fig. 5. Proposed packing of the $[Fe^{III}(L)_2]^+$ cations in compound **1**.

The magnetic behavior of compound **2** reflected by the temperature dependencies of I and $I \times T$ product of the whole EPR spectrum is shown in Fig. 9. One can see that the temperature dependence of I reaches its maximum at 10.2 K (Fig. 9a) and then decreases monotonically. The temperature variation of $I \times T$ product (Fig. 9b) demonstrates a behavior similar to μ_{eff} (Fig. 1b): a sharp decrease below 30 K, practically a plateau from 30 to 150 K, and a gradual increase above 150 K.

In order to understand the nature of the observed anomalies, the temperature dependencies of the EPR lines integrated intensity were examined for each type of iron(III) centers separately. The analysis of the EPR signals for the each type of iron centers was carried out in a similar way as for complex **1**. The simulated EPR spectra shown in Fig. 8 (see dashed lines) are calculated with magnetic parameters: $g = 2.0$, $D = 0.42\ cm^{-1}$, $E = 0.1\ cm^{-1}$ for HS and $g_\perp = 2.21$, $g_\parallel = 1.93$ for LS centers. As can be seen, a satisfactory agreement is obtained between the experimental and theoretical spectra.

Now let us analyze the EPR spectra behavior of each type of Fe (III) centers independently. Fig. 10 shows the temperature variation of the EPR integrated intensity (I) for HS (I_{HS}) and LS (I_{LS}) centers. Both I_{HS} and I_{LS} demonstrate a sharp maximum at $T_N = 10.2$ K and above T_N follow the Curie-Weiss law up to 150 K with constants $\theta_1 = -7.8$ K and $\theta_2 = -9.8$ K for HS and LS centers, respectively.

The appearance of maximum on the curves indicates that LS iron centers as well as HS ones are coupled by antiferromagnetic (AF) exchange interactions. In accordance with the EPR integrated intensities, the number of LS and HS centers is about 77% and 23% at $T_N = 10.2$ K, respectively. If we normalize the maximum values of the EPR integrated intensity of each fraction per unit and superimpose these curves, then an almost identical magnetic behavior is observed (Fig. 11a) for HS and LS centers up to 150 K. This fact indicates that iron(III) ions are linked into dimers. Above 150 K the temperature dependencies of I_{HS} and I_{LS} deviate from the Curie-Weiss law: the number of HS centers increases, while the number of LS centers decreases relative to the Curie-Weiss law. Such a behavior indicates that a partial SCO takes place in compound **2** between 150 and 300 K.

Thus, we can conclude that the counterion has a significant impact on the magnetic properties of the $[Fe(L)_2]^+$ complexes. The ability of the anion to form an effective network of hydrogen bonds and its size define the packing motif of the $[Fe(L)_2]^+$ complexes and the structure of ionic bilayers. The chlorine and hexafluorophosphate anions are able to form a network of hydrogen bonds with the amine groups of the ligands and thus can produce a bilayered packing with a chain structure of ionic bilayers (Fig. 5). A closer packing within the chains occurs in case of chlorine anions, which have a smaller size. The formation of a chain structure of ionic bilayers gives rise to intrachain interactions within the bilayers (more effective in case of chlorine anions), and thus a low-dimensional magnetic structure is formed. A small anion, as known [50], stabilizes the HS state, and exchange interactions within the chain completely annihilate the spin transition as observed in compound **1**. The perchlorate anions form stronger hydrogen bonds with the amine hydrogens, but the increase in counterion size favours the formation of a dimeric structures (Fig. 11b). This conclusion is in line with the results of DFT calculations (see Section 2.4 for details). Such a modification of the network of exchange interaction in compound **2** is responsible for the appearance of a partial spin transition of the Fe(III) centers.

2.4. Quantum-chemical calculations

Since two flexible tridentate ligands can coordinate to a metal ion in three different ways, a series of DFT calculations was performed to assign the structure of coordination core in the $[Fe(SalEen)_2]^+$ complex and its dendrimeric analogue. According to the calculations, the ligands adopt a meridional coordination mode (a *mer* isomer shown in Fig. 12 is energetically most preferable in both cases). For the $[Fe(SalEen)_2]^+$ complex, the other two isomers are higher in energy by 28.8 and 23.0 $kJ \cdot mol^{-1}$. For the dendrimeric complex, the energy difference between the conformations within the dendritic tails (for any coordination model) does not exceed 40.5 $kJ \cdot mol^{-1}$, and the energy of the most stable *mer* structure is lower by about 40–50 $kJ \cdot mol^{-1}$ than that of the most stable structures of the other two coordination models.

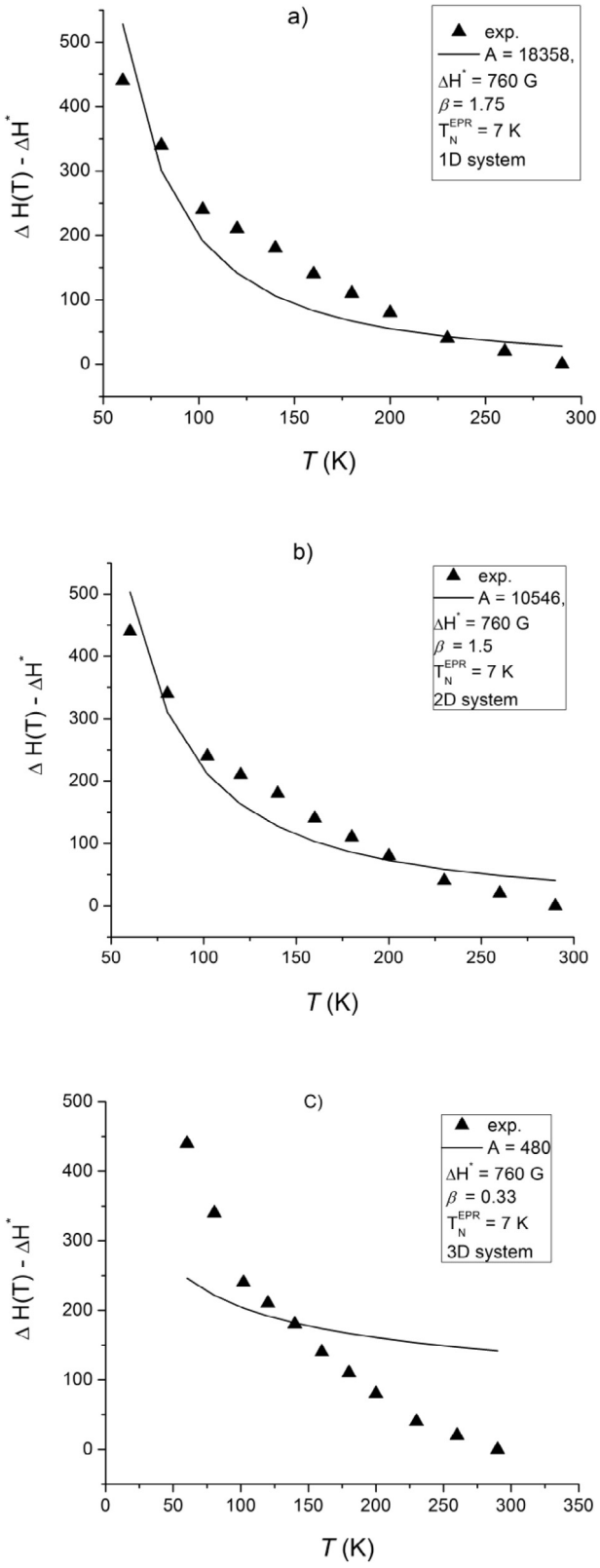

Fig. 6. Temperature dependencies of the EPR line width (ΔH) of the broad line derived from the fitting in accordance with Eq. (2). The solid lines are the approximation of $\Delta H(T)$ dependence with $\beta = 1.5$ (*a*), $\beta = 1.75$ (*b*) and $\beta = 0.33$ (*c*).

In the *mer* coordination polyhedron, the N(H) donor atoms occupy the neighboring positions, and the amine hydrogens are not locked by the dendritic tails. Such a model of coordination

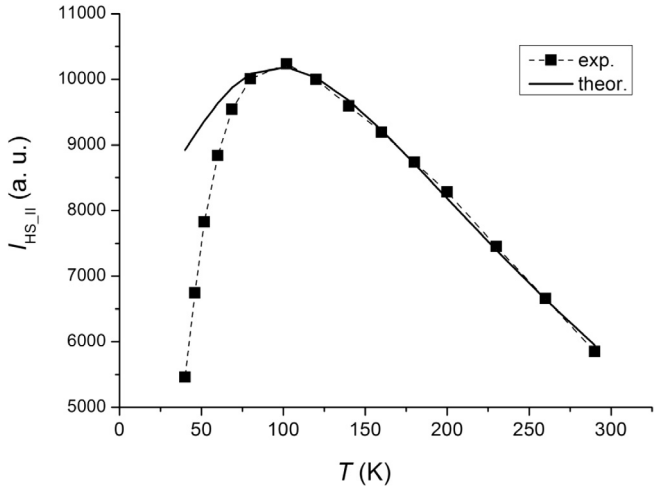

Fig. 7. Temperature dependence of I_{HS_II} versus T for **1**. Solid line represents the best fit according to Eq. (4).

polyhedron allows the formation of dimeric ensembles or chains, where neighboring complexes are linked by hydrogen bonds between the amine hydrogens and the counterions. To examine such a possibility, we performed a series of DFT calculations for dimeric ensembles comprising two complexes and two counterions. We considered both the two identical enantiomers of the complex and the enantiomer pair (Fig. 12). Different initial orientations of the ensemble components were considered, and, as a result, a set of equilibrium structures was obtained. Among these structures, the most stable one is formed by the enantiomer pair (Fig. 13). One can see that enantiomers are shifted to reduce the steric repulsion between the ethyl groups. By defining this unit as an elementary unit, we proposed a chain structure of ionic bilayers in compound **1** (Fig. 5). In case of perchlorate anions, the network of intermolecular hydrogen bonds in the optimized structure of analogous dimeric ensemble is more compact that is indicative of the strengthening of supramolecular hydrogen bonds (Fig. 13). The latter in conjunction with the increase in the counterion size explains the formation of dimeric structures in compound **2** (Fig. 11b).

3. Conclusions

EPR spectroscopy and static magnetic susceptibility measurements have been used to study the magnetism of two novel Fe(III) dendrimeric complexes of the second generation, namely $[Fe(L)_2]^+X^-$ (X = Cl^- (**1**), ClO_4^- (**2**); L = 3,5-di(3,4,5-tris(tetradecyloxy) benzoyloxy) benzoyl-4-oxy-salicylidene-N′-ethyl-*N*-ethylenediamine), and the influence of the counterion on the structure and the spin-transition properties. Iron(III) ions have a pseudooctahedral N_4O_2 coordination core in these compounds. EPR data show that compound **1** contains about 98% of high-spin (HS, $S = 5/2$) and ~ 2% of low-spin (LS, $S = 1/2$) Fe(III) centers. The HS Fe(III) centers are characterized by a broad EPR line at $g \approx 2$, whose integrated intensity passes through a broad maximum at $T_{max} \approx 100$ K in the temperature range (300–30 K) and indicates the formation of short-range correlation effects. The value of the critical exponent $\beta = 1.5$ describing the anomalous broadening of this EPR line at low temperatures indicates the quasi-two-dimensional antiferromagnetic nature of magnetism in complex **1**. It has been shown that cationic iron(III) complexes are packed in chains forming ionic bilayers, and exchange interactions within the chain completely annihilate the spin transition in compound

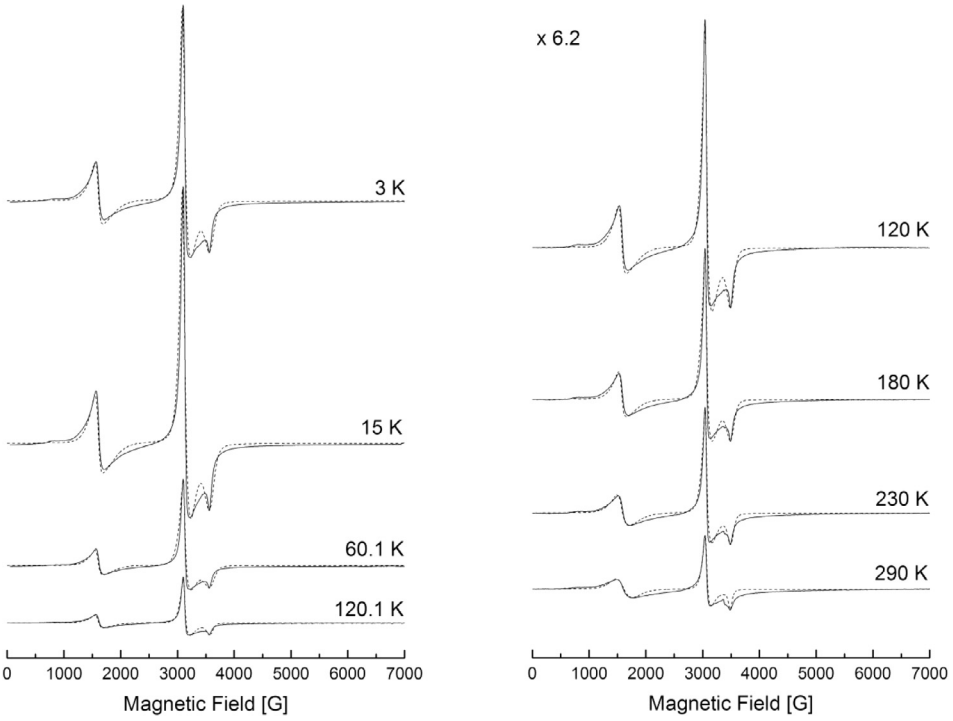

Fig. 8. Temperature profile of the EPR spectra of compound **2** with ClO_4^- counterion. The dashed lines show the theoretical spectra. Spectra in the temperature range (120–290 K) are recorded at higher amplification (×6.2) in comparison with spectra in the range (3–120.1 K).

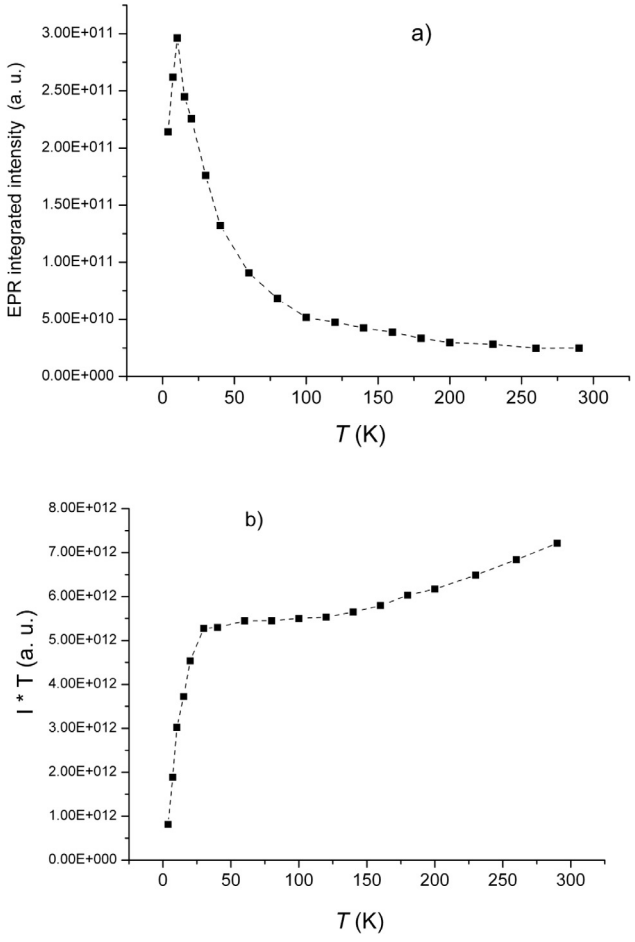

Fig. 9. (a) The temperature dependence of the EPR lines integrated intensity of the whole EPR spectrum of complex **2**. (b) The $I \times T$ vs. T plot.

1. EPR results show that compound **2** contains about 77% of LS and 23% of HS Fe(III) centers at T_N = 10.2 K. It undergoes a partial SCO (S = 1/2 ↔ 5/2) of the Fe(III) centers above 150 K and the AF ordering below 10.2 K. In this compound, iron(III) ions are linked into dimers. Our results have shown that the counterion can provide or suppress a short-range interactions between the cationic Fe (III) complexes and thus defines the magnetic structure of the compound, but exchange interactions within the chain can annihilate the spin transition.

4. Experimental

4.1. Samples preparation and characterization

*4.1.1. Synthesis of bis[3,4,5-tri(tetradecyloxy)benzoyloxybenzoyl-4-oxy-salicylidene-N′-ethyl-N-ethylenediamine]iron(III) chloride (**1**)*

A weighed portion of 3,5-di[3,4,5-tris(tetradecyloxy)benzoyloxy]benzoyl-4-oxy-2-hydroxybenzaldehyde (0.9 g) was dissolved in benzene (6 ml). Then N′-ethyl-*N*-ethylenediamine (0.09 g) dissolved in dry ethanol (10 ml) was added, stirred for 5 min. After adding an alcohol solution of KOH (0.113 g, 10 ml), we added slowly, dropwise, a solution of $FeCl_3$ (0.083 g) in ethanol, stirred for 4 h, filtered with a glass filter (porous 4), washed with cold ethyl alcohol and dry ethyl ether, and reprecipitated from a mixture of dried benzene–ethanol (1/6) solvents. The residue was dissolved in benzene and then filtered through Teflon mesh PTFE filters (0.200 μ). The desired product was isolated by freeze drying from benzene solution. The product was a fine solid dark brown powder. Yield is 0.89 g.

Found, %: C, 71.58; H, 10.79; N, 2.32; O, 9.60. Calc. for $C_{120}H_{206}N_4O_{12}Fe{\cdot}Cl$, %: C, 72.49; H, 10.44; N, 2.82; O, 9.66.

IR spectrum of the complex, ν_{max}/cm^{-1}: 3078.75 w (C–H), 2920, 2852 s (–$(CH_2)_n$–CH_3), 1730 s (C═O), 1630 s (C═N), 1191, 1118 s (Alk–C–O–C(Ph)), 988 s (NH).

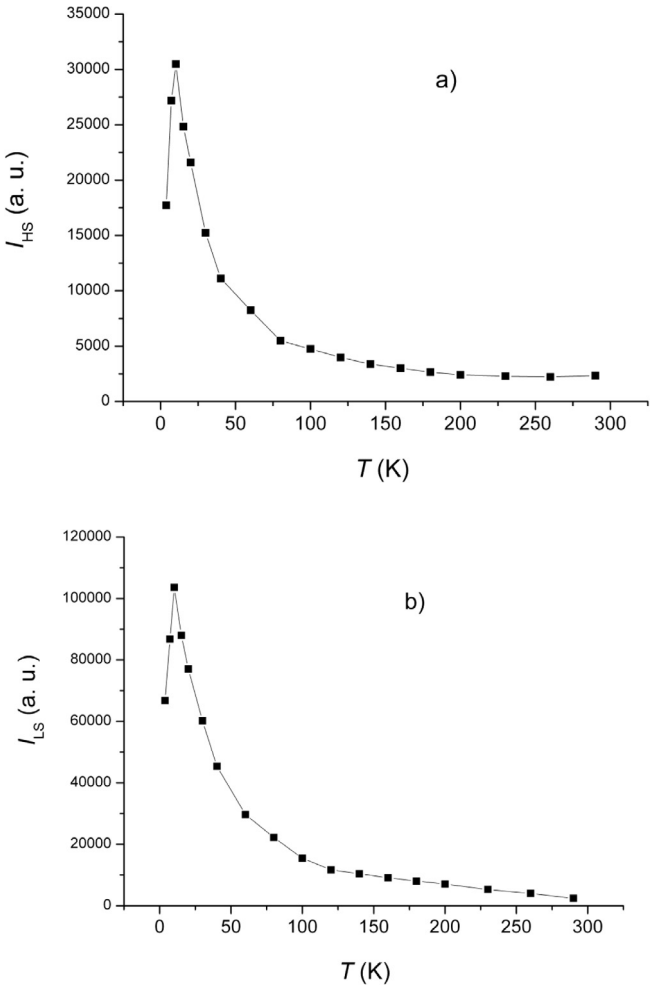

Fig. 10. The temperature dependencies of the EPR lines integrated intensity of the HS (a) and the LS (b) iron(III) centers of the compound **2**.

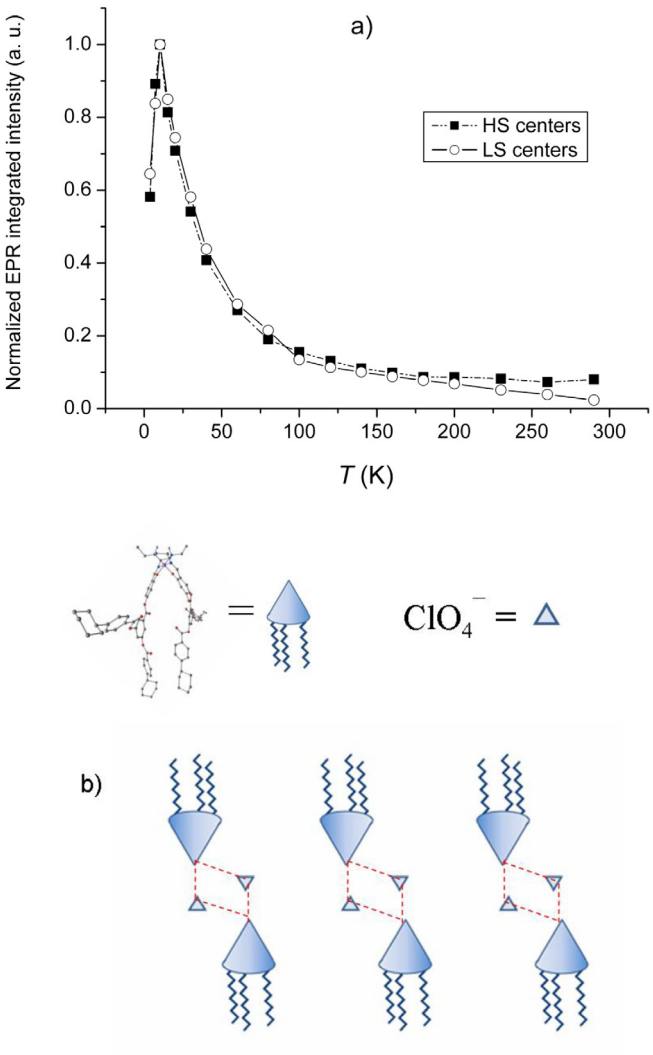

Fig. 11. Temperature dependences of the EPR integrated intensities normalized per unit of the HS and LS centers at $4.2 \leq T \leq 300$ K (*a*). Proposed packing of the $[Fe^{III}(L)_2]^+$ cations in complex **2** (*b*).

*4.1.2. Synthesis of bis[3,4,5-tri(tetradecyloxy)benzoyloxybenzoyl-4-oxy-salicylidene-N′-ethyl-N-ethylenediamine]iron(III) perchlorate (**2**)*

The synthesis was similar to that of complex (**1**). In 15 min after adding an alcohol solution of $Fe(NO_3)_3 \cdot 9H_2O$ (0.21 g), we added a weighed portion of $NaClO_4$ (0.249 g) dissolved in ethanol. The synthesis continued for 6 h. The precipitate was filtered with a glass filter, washed with ethyl alcohol, reprecipitated from a mixture of dried benzene–ethanol (1/6) solvents The residue was dissolved in benzene and then filtered through Teflon mesh PTFE filters (0.200 μ). The desired product was isolated by freeze drying from a benzene solution. The product was fine solid dark brown powder. Yield is 1.05 g.

Found, %: C, 69.86; H, 9.50; N, 2.14; O, 13.67. Calc. for $C_{120}H_{206}N_4O_{12}Fe \cdot ClO_4$, %: C, 70.29; H, 10.03; N, 2.73; O, 12.48.

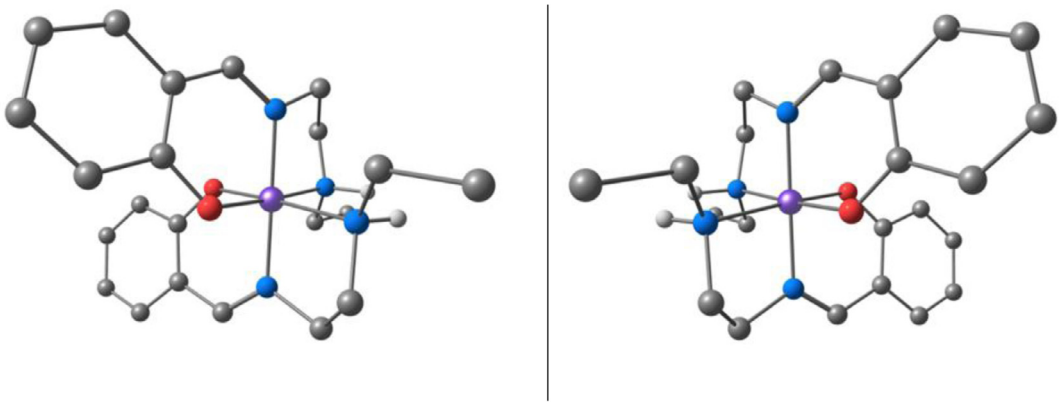

Fig. 12. Two enantiomers (*mer* structures) of the cationic complex. Only amine hydrogens are shown, dendritic tails are omitted.

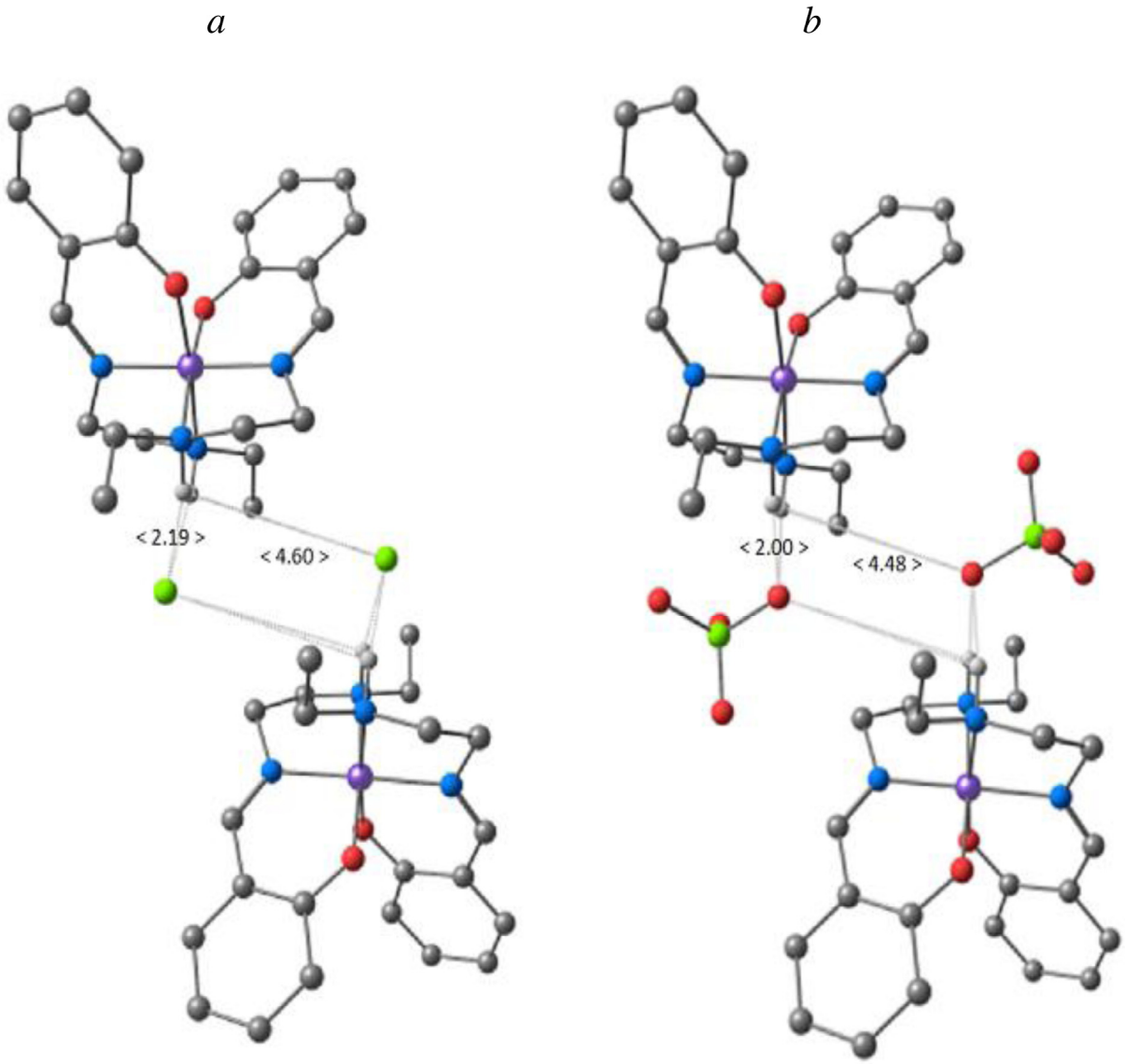

Fig. 13. Dimeric ensembles formed by the enantiomer pair and the chlorine (*a*) or perchlorate (*b*) anions. Only amine hydrogens are shown, dendritic tails are omitted. Averaged distances are given in Å.

IR spectrum of the complex, ν_{max}/cm^{-1}: 3265 s (NH), 3100, 2975 m (Ph–H), 2925, 2852 s (–(CH2)n–CH3), 1733 s(C=O), 1628 s (C=N), 1193 s (Alk–C–O–C(Ph)), 1115 s (ClO4−) and 989 m (NH).

4.2. Physical measurements

The EPR experiments were carried out on the powder sample. EPR studies were performed using X-band (9.41 GHz) CW-EPR EMXplus Bruker spectrometer that was provided with the helium ER 4112HV and the digital ER 4131VT temperature control systems. The accuracy of the reported magnetic parameters for LS iron complexes was $\Delta g = \pm 0.005$ and ±0.005 for the fine structure parameters. The error in the measurement of the EPR lines integrated intensity was ~4–5%. Magnetic susceptibility measurements of the polycrystalline samples was measured at heating rates of 2 K min^{-1} in a 0.1 T magnetic field by means of a Quantum Design MPMSXL SQUID magnetometer at temperatures of 4.2–300 K. The paramagnetic components of magnetic susceptibility χ were determined with allowance for the diamagnetic contribution evaluated from Pascal's constants.

4.3. Quantum-chemical calculations

All geometry optimizations were carried out using spin-unrestricted DFT as implemented in the ORCA program (version 3.0.3) [51]. The hybrid B3LYP [52,53] and X3LYP (for better description of noncovalent interactions) [54] functionals were used in single-complex and dimeric-ensemble cases, respectively, in conjunction with the TZVP basis set [55]. The RIJCOSX approximation [56] and the increased integration grid (Grid4) were used throughout.

Acknowledgment

We gratefully acknowledge the financial support for this work by RAS Presidium program No. 24 and grant of Russian Foundation for Basic Research (RFBR) № 14-03-31280-mol_a.

References

[1] M.A. Halcrow (Ed.), Spin-Crossover Materials: Properties and Applications, John Wiley & Sons, Ltd., Chicheser, 2013.
[2] P. Gütlich, A.B. Gaspar, Y. Garcia, Beilstein J. Org. Chem. 9 (2013) 342–391.
[3] P. Gütlich, H.A. Goodwin, Top. Curr. Chem. 233 (2004) 1–47.
[4] A. Hauser, Top. Curr. Chem. 234 (2004) 155–198.
[5] V. Ksenofontov, A.B. Gaspar, P. Gütlich, Top. Curr. Chem. 235 (2004) 23–64.
[6] J.-F. Letard, J. Mater. Chem. 16 (2006) 2550–2559.
[7] A. Cannizzo, C.J. Milne, C. Consani, W. Gawelda, C. Bressler, F. Van Mourik, M. Chergui, Coord. Chem. Rev. 254 (2010) 2677–2686.
[8] Y. Bodenthin, G. Schewarz, Z. Tomkowicz, M. Lommel, T. Geue, W. Haase, H. Möhwald, U. Pietsch, D.G. Kurth, Coord. Chem. Rev. 253 (2009) 2414–2422.
[9] R.-J. Wie, J. Tao, R.-B. Huang, L.-S. Zheng, Eur. J. Inorg. Chem. 2013 (2013) 916–926.
[10] S. Heider, H. Petzold, G. Teucher, Eur. J. Inorg. Chem. 2013 (2013) 2382–2388.
[11] D.J. Harding, P. Harding, W. Phonsri, Coord. Chem. Rev. 313 (2016) 38–61.
[12] P. Gütlich, Y. Garcia, H.A. Goodwin, Chem. Soc. Rev. 29 (2000) 419–427.
[13] O. Kahn, Nature 399 (1999) 21–22.
[14] Y. Einaga, J. Photochem. Photobiol. C: Photochem. Rev. 7 (2006) 69–88.
[15] O. Sato, J. Photochem. Photobiol. C: Photochem. Rev. 5 (2004) 203–223.
[16] M.A. Halcrow, Chem. Lett. 43 (2014) 1178–1188.
[17] S. Brooker, Chem. Soc. Rev. 44 (2015) 2880–2892.
[18] P.J. van Koningsbruggen, Y. Maeda, H. Oshio, Coord. Chem. Rev. 233 (2004) 259–324.
[19] M. Nihei, T. Shiga, Y. Maeda, H. Oshio, Coord. Chem. Rev. 251 (2007) 2606–2621.
[20] P. Guionneau, Dalton Trans. 43 (2014) 382–393.
[21] A. Bousseksou, G. Molnar, L. Salmon, W. Nicolazzi, Chem. Soc. Rev. 40 (2011) 3313–3335.
[22] G. Aromi, L.A. Barros, O. Roubeau, P. Gamez, Coord. Chem. Rev. 255 (2011) 485–546.
[23] O. Roubeau, Chem. Eur. J. 18 (2012) 15230–15244.
[24] C. Janiak, Dalton Trans. (2003) 2781–2804.
[25] V. Percec, M. Glodde, T.K. Bera, Y. Miura, I. Shiyanovskaya, K.D. Singer, V.S.K. Balagurusamy, P.A. Heiney, I. Schnell, A. Rapp, H.-W. Spiess, S.D. Hudson, H. Duan, Nature 419 (2002) 384–387.
[26] J.I. Paez, M. Martinelli, V. Brunetti, M.C. Strumia, Polymers 4 (2012) 355–395.
[27] N.E. Domracheva, A.V. Pyataev, V.E. Vorobeva, E.M. Zueva, J. Phys. Chem. B 117 (2013) 7833–7842.
[28] C.-F. Sheu, S.-M. Chen, G.-H. Lee, Y.-H. Liu, Y.-S. Wen, J.-J. Lee, Y.-C. Chuang, Y. Wang, Eur. J. Inorg. Chem. 2013 (2013) 894–901.
[29] P. Gütlich, A. Hauser, H. Spiering, Angew. Chem. 106 (1994) 2109–2141.
[30] P. Gütlich, A. Hauser, H. Spiering, Angew. Chem. Int. Ed. Engl. 33 (1994) 2024–2054.
[31] S. Hayami, S. Miyazaki, M. Yamamoto, K. Hiki, N. Motokawa, A. Shuto, K. Inoue, T. Shinmyozu, Y. Maeda, Bull. Chem. Soc. Japn. 79 (2006) 442–450.
[32] M.S. Haddad, M.W. Lynch, W.D. Federer, D.N. Hendrickson, Inorg. Chem. 20 (1981) 123–131.
[33] N. Domracheva, V. Vorobeva, A. Pyataev, R. Tamura, K. Suzuki, M. Gruzdev, U. Chervonova, A. Kolker, Inorg. Chim. Acta 439 (2016) 186–195.
[34] U.V. Chervonova, M.S. Gruzdev, A.M. Kolker, O.B. Akopova, J. Struct. Chem. 57 (2016) 478–490.
[35] U.V. Chervonova (Ph.D. thesis), G.A. Krestov Institute of Solution Chemistry of RAS, Ivanovo, 2012.
[36] M. Gruzdev, U. Chervonova, O. Akopova, A. Kolker, J. Chem. Sci. 127 (2015) 1801–1810.
[37] A.P. Summerton, A.A. Diamantis, M.R. Snow, Inorg. Chim. Acta 27 (1978) 123–128.
[38] N. Domracheva, V. Vorobeva, A. Pyataev, A. Ivanova, Appl. Magn. Reson. 47 (8) (2016) 903–913.
[39] H. Wickman, M. Klein, D. Shirley, J. Chem. Phys. 42 (1965) 2113–2117.
[40] R. Aasa, J. Chem. Phys. 52 (1970) 3919–3930.
[41] P.S. Berdonosov, E.S. Kuznetsova, V.A. Dolgikh, A.V. Sobolev, I.A. Presniakov, A. V. Olenev, B. Rahaman, T. Saha-Dasgupta, K.V. Zakharov, E.A. Zvereva, O.S. Volkova, A.N. Vasiliev, Inorg. Chem. 53 (2014) 5830–5838.
[42] D.L. Huber, Phys. Rev. B 6 (1972) 3180–3186.
[43] K. Kawasaki, Prog. Theor. Phys. 39 (1968) 285–311.
[44] H. Mori, K. Kawasaki, Prog. Theor. Phys. 28 (1962) 971–987.
[45] M. Fisher, Am. J. Phys. 32 (1964) 343–346.
[46] R. Dingle, M.E. Lines, S.L. Holt, Phys. Rev. 187 (1969) 643–648.
[47] T. Oguchi, Phys. Rev. 133 (1964) A1098.
[48] N. Guskos, G. Zolnierkiewicz, J. Typek, R. Szymczak, A. Blonska-Tabero, Mater. Sci.-Poland 30 (2012) 1–9.
[49] A.A. Katanin, V.Yu. Irkhin, Physics-Uspekhi 50 (2007) 613–637.
[50] M. Yamada, M. Ooidemizu, Y. Ikuta, S. Osa, N. Matsumoto, S. Iijima, M. Kojima, F. Dahan, J.-P. Tuchagues, Inorg. Chem. 42 (2003) 8406–8416.
[51] F. Neese, WIREs Comput. Mol. Sci. 2 (2012) 73–78.
[52] A.D. Becke, J. Chem. Phys. 98 (1993) 5648–5652.
[53] P.J. Stephens, F.J. Devlin, C.F. Chabalowski, M.J. Frisch, J. Phys. Chem. 98 (1994) 1623–11627.
[54] X. Xu, W.A. Goddard III, Proc. Natl. Acad. Sci. U.S.A. 101 (2004) 2673–2677.
[55] A. Schafer, H. Horn, R. Ahlrichs, J. Chem. Phys. 100 (1994) 5829–5835.
[56] F. Neese, F. Wennmohs, A. Hansen, U. Becker, Chem. Phys. 346 (2009) 98–109.